Letters in Applied NanoBioScience
Open-Access Journal (ISSN: 2284-6808)

Article
Volume 13, Issue 3, 2024, 124
https://doi.org/10.33263/LIANBS133.124

A Density Functional Theory Study on the Adsorption of Methyl Mercury and Arsenous Acid on Cellulose Chain

Art Anthony Z. Munio [1,2,3], Alfredo Q. Liboon Jr [2,3,*], Yhebron J. Lagud [2], Alvanh Alem G. Pido [3,4], Lorymer L. Jauculan [2]

1. Physics Department, Mindanao State University–Iligan Institute of Technology, 9200 Iligan City, Philippines; artanthony.munio@g.msuiit.edu.ph (A.A.Z.M.), leocristobal.ambolode@g.msuiit.edu.ph (L.C.C.A);
2. Jose Rizal Memorial State University–Zamboanga del Norte, Philippines; alfredoliboonjr@jrmsu.edu.ph; artanthonymunio@jrmsu.edu.ph (A.A.Z.M.);
3. Premier Research Institute of Science and Mathematics (PRISM), Mindanao State University–Iligan Institute of Technology, 9200 Iligan City, Philippines;
4. Physics Department, Mindanao State University-Main Campus, 9700 Marawi City, Philippines; alvanhalem.pido@msumain.edu.ph (AAGP);

* Correspondence: alfredoliboonjr@jrmsu.edu.ph (A.Q.L.);

Scopus Author ID: 57810089600

Received: 28.06.2023; Accepted: 23.11.2023; Published: 26.07.2024

Abstract: Methyl mercury (MeHg) and arsenous acid (H_3AsO_3) are toxic chemicals that pollute freshwater sources. Driven by this environmental concern, developing efficient, eco-friendly, adsorbent materials has become necessary. Using first-principles density functional theory, we decipher the fundamental adsorption mechanism of MeHg and H_3AsO_3 on the cellulose biopolymer. The interaction is mainly described as physisorption by considering various bonding sites and orientations of MeHg and H_3AsO_3 on the cellulose chain. According to the binding energy, H_3AsO_3 interacts more strongly with cellulose than MeHg. The hydrogen bonding between H_3AsO_3 and the functional groups of cellulose plays an important role in the adsorption strength. Whereas MeHg does not form a hydrogen bond with the functional groups, the adsorption is mainly described as an induced dipole. These claims are further supported by careful analysis of the electronic redistribution via Charge Density Difference, Bader charge analysis, and Electron Localization Function. Overall, the results revealed that cellulose is a competitive material for trapping H_3AsO_3owing to its abundance in oxygen-functional groups. The findings presented here proposed the adsorption mechanism MeHg and H_3AsO_3 on the cellulose biopolymer. This work will be the basis for developing cellulose-based adsorbent material and bridging the gap in the literature.

Keywords: heavy metals; cellulose; MeHg; arsenous acid; DFT; bonding mechanism.

1. Introduction

Methyl mercury (MeHg) and arsenous acid (H_3AsO_3) are toxic substances that have well-known detrimental effects on human health and the environment [1,2]. These chemicals and hazardous compounds pollute the freshwater system due to both manufactured and natural causes [3]. MeHg is a highly toxic form of mercury that can accumulate in fish and seafood, making it easy for human intake [4]. Thus, removing MeHg from wastewater before discharging it into the environment is essential. On the other hand, H_3AsO_3 is one of the common forms of arsenic in freshwater and has severe recorded effects on human health [5]. Consumption of these chemicals greater than permitted can lead to various health problems

[6,7]. Due to these alarming reports, effective filtration methods for heavy metal compounds are a critical topic in the scientific community.

Various methodologies have been developed to remove heavy metals from water systems. Among these, the adsorption method is simpler, practical, and cost-effective [8,9]. Various candidate materials with impressive performance include metal-oxides, metal-based nanoparticles, graphene-based material, minerals, polymers, and biopolymers [10–16]. It is known that Hg and As strongly interact with other metals, as evidenced by metal nanoparticles' efficiency in trapping heavy metal ions [17–20]. However, the metal-based adsorbent can potentially cause secondary contaminants, which are also hazardous. Thus, a material with intrinsic eco-friendly properties is an ideal choice. In recent years, cellulose and its derivatives have paid much interest as candidate-based materials for water remediation technology owing to their biocompatibility, wide surface area, and rich reactive sites for trapping heavy metals [14,15,21–23]. The ability of cellulose to be hybridized with other nanomaterials makes cellulose attractive as a multifunctional adsorbent material [24]. These reasons make cellulose part of the ideal materials for the next-generation adsorbent.

Cellulose is a naturally occurring polymer widely used in various established industrial applications and emerging innovative technology [15,21,22,25–27]. Cellulose fibers have a high surface area-to-volume ratio and modest mechanical properties, are biocompatible, and are rich in oxygen functional groups [28]. These specific properties make cellulose attractive for water remediation technology. Cellulose can be modified chemically to enhance its adsorption capacity and selectivity for specific heavy metal ions [29–32]. However, the long list of heavy metals and diverse chemically modified versions of cellulose makes bonding characterization unclear. The atomistic bonding information of heavy metal compounds on cellulose and its derivatives is a prerequisite in designing an effective cellulose-based adsorbent material.

Density functional theory is one of the most versatile methods for studying chemical systems at the fundamental level. For example, Barker *et al.* [33] demonstrate that perfluorinated molecules can be adsorbed on the graphene-oxide mainly by dispersion and hydrogen bonding. Another study reported a strong metal nanocluster and H_3AsO_3 interaction, which explains the observed experimental efficiency [34]. Recently, the adsorption of MeHg and H_3AsO_3 on FeS has also been explored in the following references [35,36]. The results indicate that multiple factors, such as the phase of the FeS, highly influence the interaction's characteristics. On the other hand, biopolymers such as cellulose and their derivatives have been widely studied experimentally [37]. However, the interaction of heavy metal ions adsorption on biopolymers is rarely examined [31,38,39]. The same thing can be said about the biopolymer-heavy metal compound, where no study has been conducted on this topic. This research gap is essential in understanding the selectivity of cellulose in trapping heavy metal compounds.

In this work, we systematically study the interaction of MeHg and H_3AsO_3 with cellulose biopolymer using first-principles density functional theory (DFT). The DFT-based simulation provides essential information on the electronic description of adsorption, which helps explain and predict novel experimental results [38–44]. The computational results here indicate that MeHg adsorbed on various bonding sites of cellulose mainly due to the van der Waals force. In contrast, the cellulose-H_3AsO_3 interaction is dominantly due to hydrogen bonding. Thus, H_3AsO_3 interacts strongly compared with MeHg. However, it is further noted

that H_3AsO_3 strongly bonds with H_2O molecules, making it mobile relative to MeHg. The finding describes the trapping mechanism of cellulose with H_3AsO_3 and MeHg.

2. Materials and Methods

All calculations are conducted using first-principles DFT using Perdew-Burke-Ernzerhof exchange-correlation functionals, Optimized Norm-Conserving pseudopotentials, and plane-wave basis set [45–47]. The semi-empirical Grimme-D3 correction accounts for the dispersion [48]. The Quantum Espresso is utilized for all calculations [49,50]. The plane wave energy cutoff is set to its optimal value, 60Ry. The *SCF* energy convergence and force threshold per atom are set to 10^{-8}Ry and 10^{-4}Ry/Bohr, respectively. A *1x1x5* k-point is utilized for all calculations. In all cases, a 12Å vacuum is included to remove the long-range effect of the periodic boundary conditions.

The 2D Electron Localization Function (ELF) is calculated to observe the character of adsorption [51,52]. The strength of the interaction is quantified by the binding energy $E_{Binding}$ using the following formula,

$$E_{Binding} = E_{Total} - (E_{Cellulose} + E_{Heavy\ Metal}) \quad (1)$$

Here, E_{Total}, $E_{Cellulose}$, and $E_{Heavy\ Metal}$ are the energy of cellulose – heavy metal system, cellulose, and heavy metal, respectively. The Bader charge transfer code by Henkelman is utilized to estimate the charge transfer [53–55]. The Charge Density Difference (CDD) isosurface is calculated to visualize the charge redistribution, computed using the convention,

$$CDD = \rho_{Total} - (\rho_{Cellulose} - \rho_{Heavy\ Metals}) \quad (2)$$

The ρ_{Tota}, $\rho_{Cellulose}$, and $\rho_{Heavy\text{-}Metal}$ denote the charge of cellulose–heavy metal system, cellulose, and heavy metals, respectively.

3. Results and Discussion

The ground state configurations of cellulose, MeHg, and H_3AsO_3 are presented in Figures 1a, 1b, and 1c, respectively. To benchmark the appropriateness of the choice of functional and pseudopotentials, we compared the atomic structural parameters of cellulose, MeHg, and H_3AsO_3 in the existing literature. The length of the cellulose unit is 10.49Å in the range with experimental and computational study outputs [56–58]. The calculated optimized Hg-C bond of MeHg is 2.31Å, longer relative to DFT based on hybrid exchange-correlation functionals [59]. The As-O bond l_1, l_2, and l_3 are 1.80Å, 1.80Å, and 1.83 Å, comparable to the following reference [36].

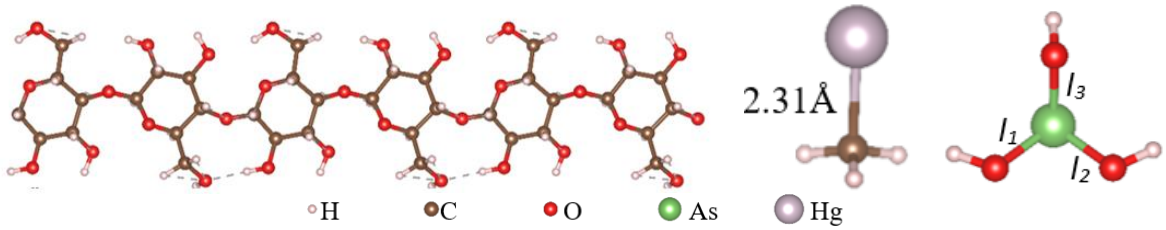

Figure 1. The optimized atomic configuration of **(a)** cellulose; **(b)** MeHg; **(c)** H_3AsO_3.

First, we evaluate the interaction of cellulose, MeHg, and H_3AsO_3 with water molecules. The optimized configuration is displayed in Figure 2. In these configurations, the average binding energy per H_2O with cellulose, MeHg, and H_3AsO_3 is -0.28eV, -0.14eV, and -0.28eV, respectively. The strength of the interaction of H_2O with cellulose is in good

agreement with the existing report [60]. It is evident in Figure 2a and Figure 2b that H_2O established a hydrogen bond with the cellulose hydroxymethyl and hydroxyl groups. Also, in Figure 2b, the H_2O molecule at the cellulose backbone points toward the oxygen, linking the cellobiose and creating hydrogen bonding. Based on Figure 2c, it is noticeable that MeHg interacts weakly with H_2O molecules. Here, the water molecules remain distant from MeHg, whereas the hydroxyl of H_3AsO_3 strongly interacts with H_2O molecules depicted in Figure 2d.

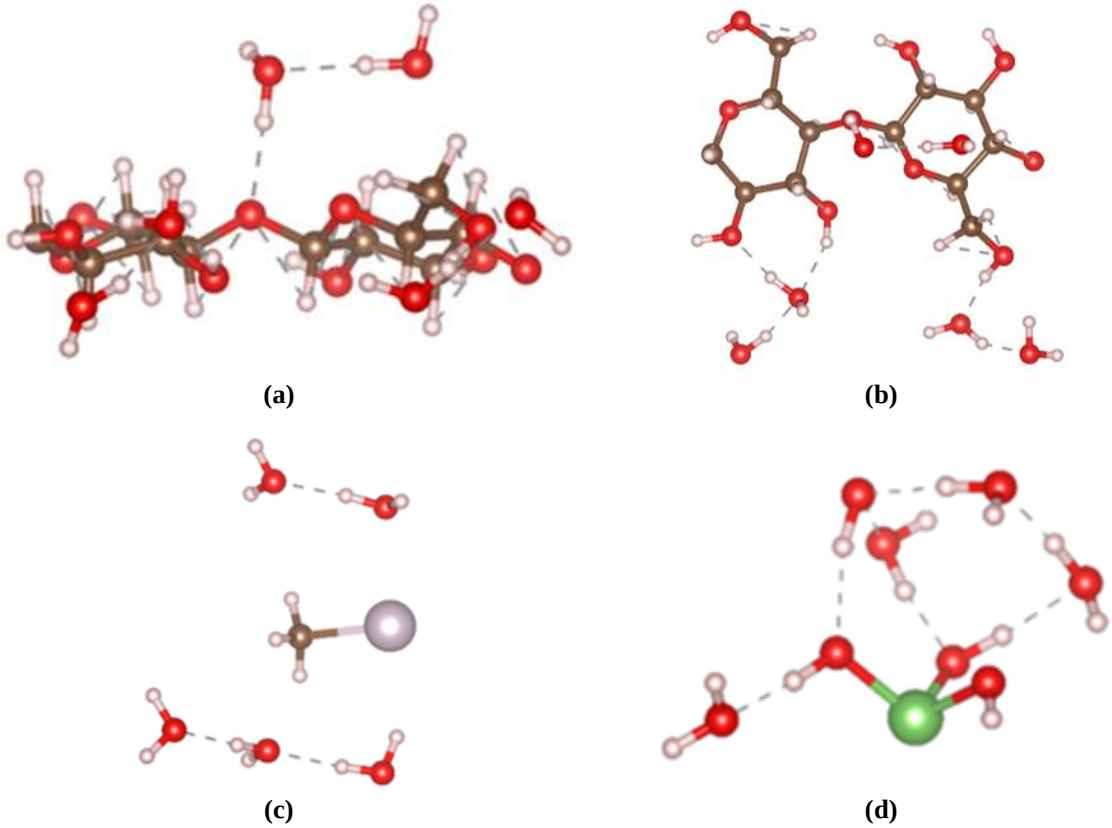

Figure 2. Cellulose with six H_2O molecules view from the **(a)** side and **(b)** top view. The optimized configuration of **(c)** MeHg and **(d)** H_3AsO_3 with five H_2O molecules.

The optimized configurations of MeHg on various cellulose sites are displayed in Figure 3. Generally, the calculated binding energy of MeHg yields a negative value, indicating a spontaneous adsorption process. It is also noted that the binding energy is larger than the thermal energy (25meV).

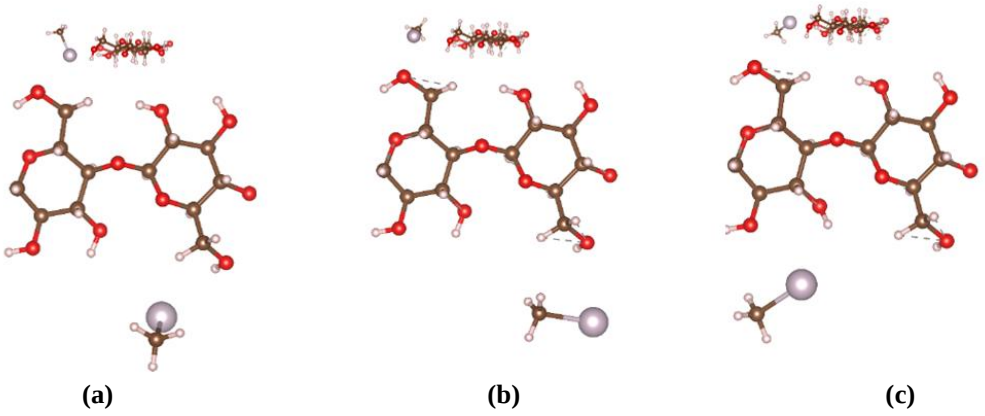

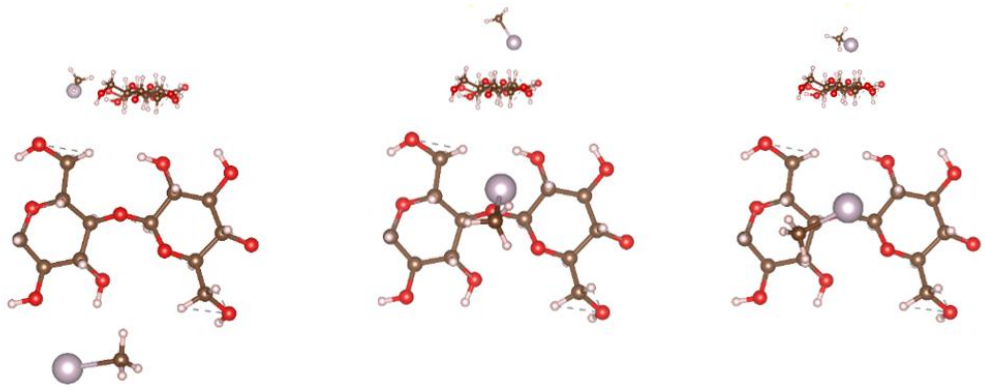

(d) (e) (f)

Figure 3. The optimized configuration of cellulose-MeHg systems. The placement of MeHg is introduced in **(a)-(b)** hydroxymethyl group; **(c)-(d)** hydroxyl groups; (**e)-(f)** cellulose's backbone.

The strength of the interaction is similar to atomic Hg adsorbed on the cellulose, yielding an average value of -0.14eV. Considering various orientations of the MeHg, either the Hg or methyl poorly interacts with the cellulose's hydroxymethyl group, hydroxyl groups, and its backbone. The binding energy is at its maximum (-0.25eV) when the interface between MeHg and cellulose is highest, as evident in Figure 3c and Figure 3f. Based on this analysis, the bonding character is mainly van der Waals type, supported by the equilibrium distances. Table 1 lists the bonding energy and equilibrium distance of the studied configurations.

Table 1. The minimum equilibrium distance, binding energy, and charge transfer of cellulose-MeHg and cellulose-H_3AsO_3 systems.

System	Min. Distance (Å)	Binding Energy (eV)
Cellulose-MeHg		
Figure 3a	3.41	-0.20
Figure 3b	2.64	-0.13
Figure 3c	2.62	-0.25
Figure 3d	2.94	-0.21
Figure 3e	3.09	-0.22
Figure 3f	3.20	-0.25
Cellulose - H_3AsO_3		
Figure 4a	2.40	-0.22
Figure 4b	1.83	-0.39
Figure 4c	1.83	-0.88
Figure 4d	1.74	-0.75
Figure 4e	1.95	-0.65
Figure 4f	2.95	-0.42

A relatively stronger interaction is observed between cellulose and H_3AsO_3, as displayed in Figure 4. It is noted that the magnitude of the binding energy is highly orientation-dependent, and the establishment of hydrogen bonds plays an important role. For instance, when the As is situated near the hydroxymethyl (Figure 4a) and cellulose's backbone (Figure 4f), the strength of the interaction is weaker by ~0.20eV compared in Figure 4b and Figure 4e where hydrogen bond(s) are formed. The strongest interaction is observed in Figure 4c (-0.88eV) when H_3AsO_3 tends to settle between hydroxymethyl and hydroxyl groups forming multiple hydrogen bonds. This is followed by Figure 4d (-0.76eV), when the H_3AsO_3 formed two hydrogen bonds with the hydroxyl groups. In Figure 4e, the hydrogen of H_3AsO_3 points toward the oxygen-linking cellulose units, yielding a binding energy of -0.65eV. In this argument, it is clear that the establishment of hydrogen bonding dictates the strength of interaction with cellulose.

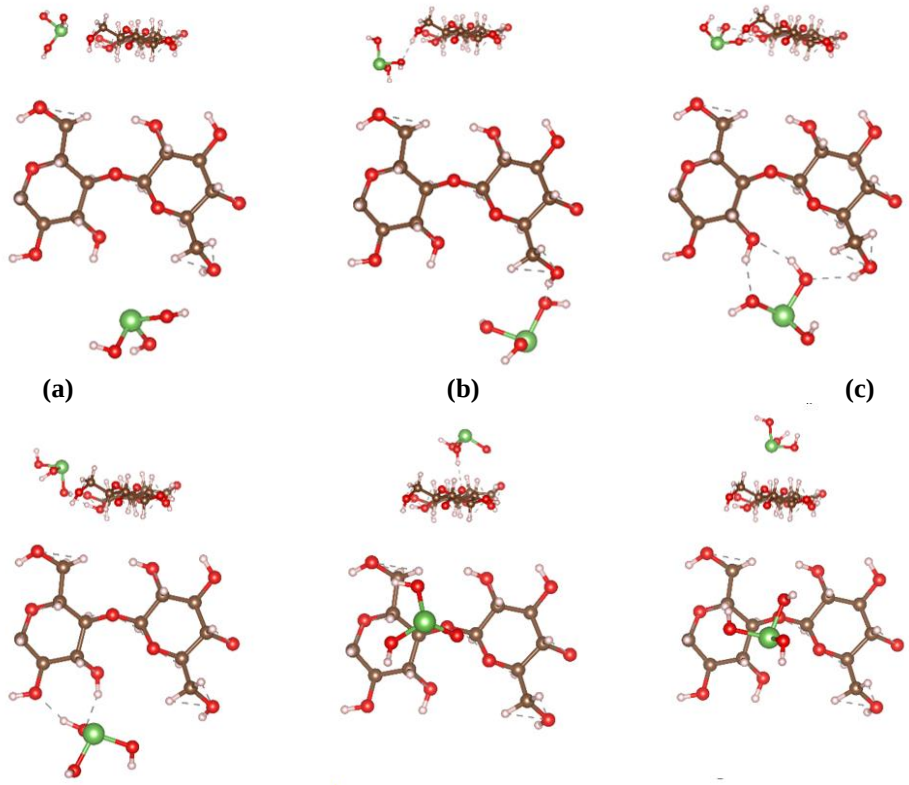

Figure 4. The cellulose-H_3AsO_3 optimized configurations. **(a)-(b)** In the H_3AsO_3 is initially placed near the hydroxymethyl; **(c)-(d)** hydroxyl groups; **(e)-(g)** cellulose's backbone.

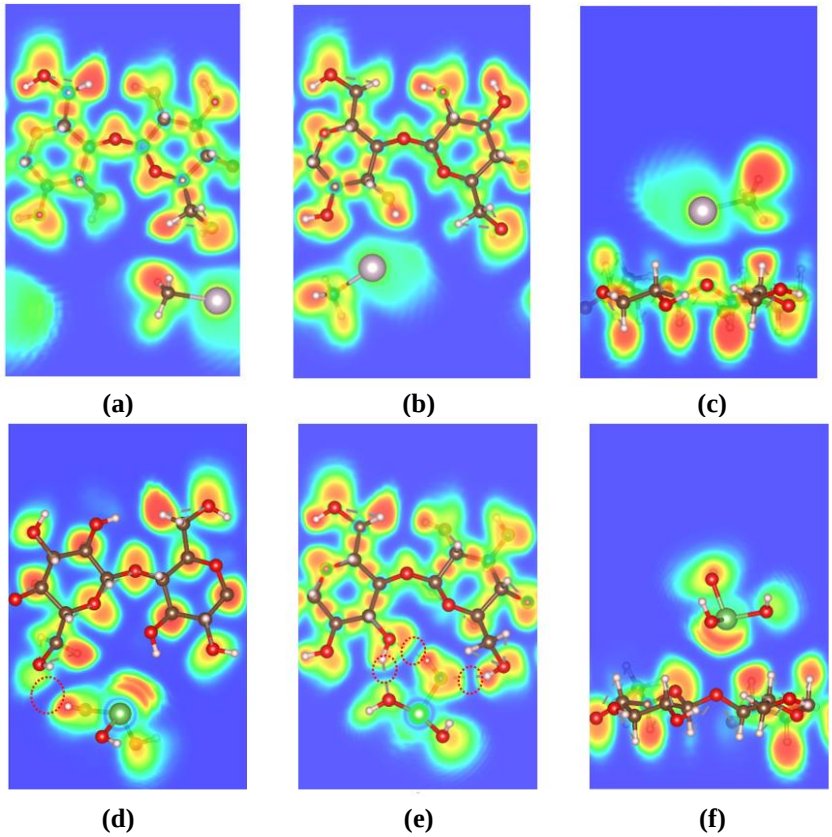

Figure 5. 2D Electron Localization Function of **(a)-(c)** cellulose-MeHg; **(d)-(f)** cellulose-H_3AsO_3. The hydrogen bond is highlighted by a red dashed line.

The 2D Electron Localization Function (ELF) of cellulose-MeHg and cellulose-H_3AsO_3 is calculated and shown in Figure 5. It is evident in Figure 5a–Figure 5c that there is

no overlapping of ELF basins between the MeHg and cellulose, indicating no sharing of electrons. However, deformed ELF means an induced dipole, which explains its weak binding energy and equilibrium distance. On the one hand, the interaction of H_3AsO_3 is mainly attributed to hydrogen bond(s) formed between the hydroxyl of H_3AsO_3 and the functional groups of cellulose, which is evident in Figure 5d and Figure 5e. The lone pair of As in the H_3AsO_3 contributes only through induced dipole, as revealed in Figure 5f.

The electronic charge redistribution of cellulose-MeHg and cellulose-H_3AsO_3 are further examined by calculating the Charge Density Difference (CDD) isosurface and quantified using Bader charge transfer analysis. Figures 6a (cellulose-MeHg) and 6b (cellulose-H_3AsO_3) give the CDD isosurface adsorbate losses 0.04e and 0.03e, respectively. Both systems have a pretty low charge transfer, a common feature of physisorption. However, significant charge redistribution is observed in the hydroxyl and hydroxymethyl groups of the cellulose in Figure 6b. The yellow and cyan isosurface indicates a redistribution of the electrons, creating more induced dipole. This case was not observed in cellulose-MeHg in Figure 6a.

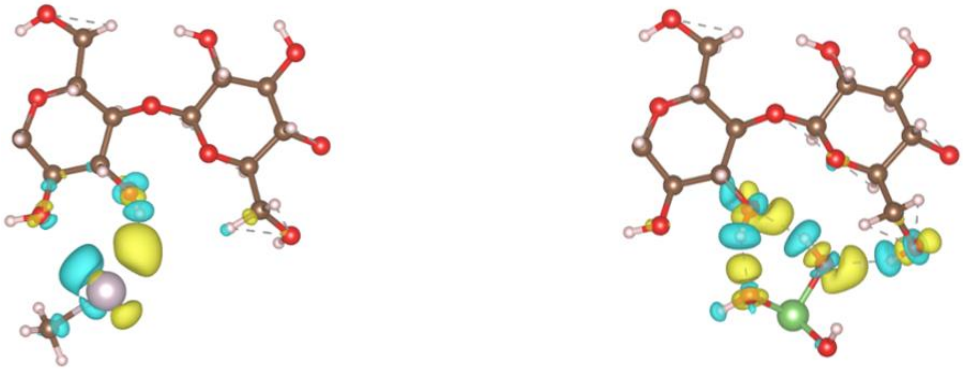

(a) **(b)**

Figure 6. Charge Density Difference (CDD) isosurface of **(a)** cellulose-MeHg; **(b)**cellulose-H_3AsO_3. The yellow and cyan isosurface indicate the accumulation and depletion of the electronic charge.

In a real system, multiple factors contribute to the interaction of adsorbent and adsorbate. For example, the interaction of MeHg and H_3AsO_3 with H_2O molecules is valuable information that dictates the likelihood that these compounds will stay in a large proportion of H_2O [33]. For the adsorbent to work optimally, the interaction of adsorbent material with adsorbate must be greater than that of adsorbate interaction with H_2O molecules. To answer this question further, reaction pathways of adsorption in water systems and molecular dynamics simulations shall be conducted in a separate study.

The electronic density of states (DOS) of the cellulose-MeHg and cellulose-H_3AsO_3 is presented in Figure 7a and Figure 7b, respectively. It is first noted that the bandgap of isolated cellulose is measured to be 5.0eV. MeHg has states appearing at the Fermi energy, showing its metallic nature. On the one hand, H_3AsO_3 has a wide-measured bandgap of 5.2eV. Generally, Figure 7a and Figure 7b indicate that the cellulose's states shifted to the higher energy relative to the Fermi energy. Moreover, Figure 7a indicates that the MeHg states remain at the Fermi level, making cellulose-MeHg metallic. The cellulose-H_3AsO_3 complex has a lower bandgap of 4.66eV compared with the isolated cellulose. The cellulose-MeHg and cellulose-H_3AsO_3 complex states can be considered a combination of their constituent counterparts. The minor difference is due to the atomic structural deformation and charge redistribution examined in the preceding discussions.

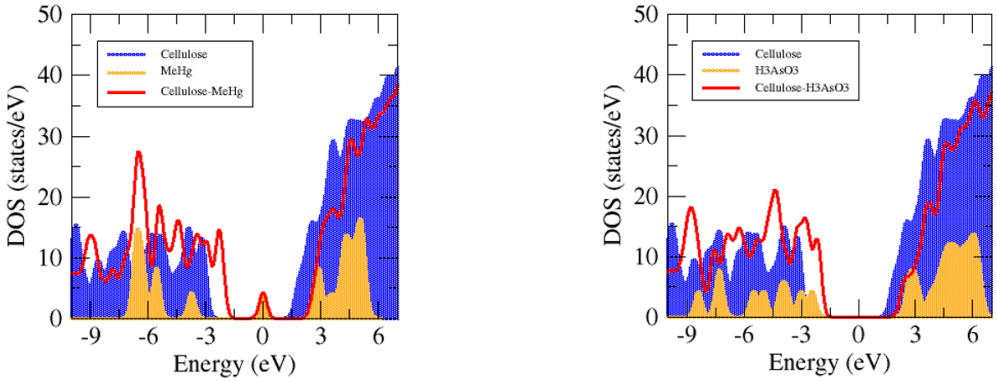

Figure 7. The electronic density of states (DOS) of **(a)** cellulose-MeHg; **(b)** cellulose- H_3AsO_3. The isolated constituents are plotted in a drop-line.

4. Conclusions

Due to the adverse health effects of MeHg and H_3AsO_3, the development of methods and materials for removing these chemicals is of significant importance. The interaction of MeHg and H_3AsO_3 with the cellulose chain is systematically examined using density functional theory with Grimme dispersion correction. MeHg and H_3AsO_3 were physisorbed on the cellulose biopolymer, where the strength of interaction of H_3AsO_3 on the cellulose chain is more robust than MeHg. Various orientations of MeHg yield almost monotonous binding energies. In contrast, H_3AsO_3 can establish multiple hydrogen bonds with the cellulose's functional groups, producing significantly higher binding energy depending on the orientation. However, it should be noted that the interaction of H_3AsO_3 with H_2O is higher than MeHg, making it prone to staying in the volume of H_2O molecules. The DOS of cellulose-MeHg and cellulose-H_3AsO_3 can be considered a superposition of the constituents. No visible hybridization and broadening of the DOS was observed, supporting the previous conclusions. The results presented here provide a fundamental understanding of the interaction of heavy metal compounds with cellulose chains. The findings provide valuable information for fabricating cellulose-based adsorbent material for heavy metals.

Funding

This research work was insitutionally funded by the Jose Rizal Memorial State University.

Acknowledgments

The authors would like to thank the office of the Campus Administrator, the Research Unit head of JRMSU-Tamilisan Campus, and the office of the Vice President for Research, Development, and Extension of JRMSU.

Conflicts of Interest

The authors declare no conflict of interest.

References

1. Al-Sulaiti, M.M.; Soubra, L.; Al-Ghouti, M.A. The Causes and Effects of Mercury and Methylmercury Contamination in the Marine Environment: A Review. *Curr. Pollution Rep.* **2022**, *8*, 249–272, http://doi.org/10.1007/s40726-022-00226-7.

2. Fatoki, J.O.; Badmus, J.A. Arsenic as an environmental and human health antagonist: A review of its toxicity and disease initiation. *J. Hazard. Mater. Adv.* **2022**, *5*, 100052, http://doi.org/10.1016/j.hazadv.2022.100052.
3. Mitra, S.; Chakraborty, A.J.; Tareq, A.M.; Emran, T.B.; Nainu, F.; Khusro, A.; Idris, A.M.; Khandaker, M.U.; Osman, H.; Alhumaydhi, F.A.; Simal-Gandara, J. Impact of heavy metals on the environment and human health: Novel therapeutic insights to counter the toxicity. *J. King Saud Univ. Sci.* **2022**, *34*, 101865, http://doi.org/10.1016/j.jksus.2022.101865.
4. Wells, E.M.; Kopylev, L.; Nachman, R.; Radke, E.G.; Congleton, J.; Segal, D. Total Blood Mercury Predicts Methylmercury Exposure in Fish and Shellfish Consumers. *Biol. Trace Elem. Res.* **2022**, *200*, 3867–3875, http://doi.org/10.1007/s12011-021-02968-9.
5. Chen, H.; Sharma, S.K.; Sharma, P.R.; Yeh, H.; Johnson, K.; Hsiao, B.S. Arsenic(III) Removal by Nanostructured Dialdehyde Cellulose–Cysteine Microscale and Nanoscale Fibers. *ACS Omega* **2019**, *4*, 22008–22020, http://doi.org/10.1021/acsomega.9b03078.
6. Rafique, M.; Hajra, S.; Tahir, M.B.; Gillani, S.S.A.; Irshad, M. A A review on sources of heavy metals, their toxicity and removal technique using physico-chemical processes from wastewater. *Environ. Sci. Pollut. Res.* **2022**, *29*, 16772–16781, http://doi.org/10.1007/s11356-022-18638-9.
7. Tchounwou, P.B.; Yedjou, C.G.; Patlolla, A.K.; Sutton, D.J. Heavy Metals Toxicity and the Environment. In Molecular, Clinical and Environmental Toxicology. Experientia Supplementum, Luch, A., Eds.; Springer, Basel, **2012**, Volume 101, 133–164, http://doi.org/10.1007/978-3-7643-8340-4_6.
8. Samavati, Z.; Samavati, A.; Goh, P.S.; Ismail, A.F.; Abdullah, M.S. A comprehensive review of recent advances in nanofiltration membranes for heavy metal removal from wastewater. *Chem. Eng. Res. Des.* **2023**, *189*, 530–571, http://doi.org/10.1016/j.cherd.2022.11.042.
9. Punia, P.; Bharti, M.K.; Dhar, R.; Thakur, P.; Thakur, A. Recent Advances in Detection and Removal of Heavy Metals from Contaminated Water. *ChemBioEng Rev.* **2022**, *9*, 351–369, http://doi.org/10.1002/cben.202100053.
10. Arora, R. Adsorption of Heavy Metals–A Review. *Mater. Today: Proc.* **2019**, *18*, 4745–4750, http://doi.org/10.1016/j.matpr.2019.07.462.
11. Qasem, N.A.A.; Mohammed, R.H.; Lawal, D.U. Removal of heavy metal ions from wastewater: a comprehensive and critical review. *npj Clean Water* **2021**, *4*, 36, http://doi.org/10.1038/s41545-021-00127-0.
12. Rajendran, S.; Priya, A.K.; Kumar, P.S.; Hoang, T.K.A.; Sekar, K.; Chong, K.Y.; Khoo, K.S.; Ng, H.S.; Show, P.L. A critical and recent developments on adsorption technique for removal of heavy metals from wastewater-A review. *Chemosphere* **2022**, *303*, 135146, http://doi.org/10.1016/j.chemosphere.2022.135146.
13. Anderson, A.; Anbarasu, A.; Pasupuleti, R.R.; Manigandan, S.; Praveenkumar, T.R.; Kumar, J.A. Treatment of heavy metals containing wastewater using biodegradable adsorbents: A review of mechanism and future trends. *Chemosphere* **2022**, *295*, 133724, http://doi.org/10.1016/j.chemosphere.2022.133724.
14. Ahankari, S.; George, T.; Subhedar, A.; Kar, K.K. Nanocellulose as a sustainable material for water purification. *SPE Polymers* **2020**, *1*, 69–80, http://doi.org/10.1002/pls2.10019.
15. Mautner, A. Nanocellulose water treatment membranes and filters: a review. *Polym. Int.* **2020**, *69*, 741–751, http://doi.org/10.1002/pi.5993.
16. Mohammadnezhad, G.; Behbahan, A.K. Polymer matrix nanocomposites for heavy metal adsorption: a review. *J. Iran Chem. Soc.* **2020**, *17*, 1259–1281, http://doi.org/10.1007/s13738-020-01864-8.
17. Mahmoud, A.M.; Ibrahim, F.A.; Shaban, S.A.; Youssef, N.A. Adsorption of heavy metal ion from aqueous solution by nickel oxide nano catalyst prepared by different methods. *Egypt. J. Pet.* **2015**, *24*, 27–35, http://doi.org/10.1016/j.ejpe.2015.02.003.
18. Yadav, N.; Singh, S.; Saini, O.; Srivastava, S. Technological advancement in the remediation of heavy metals employing engineered nanoparticles: A step towards cleaner water process. *Environ. Nanotechnol. Monit. Manag.* **2022**, *18*, 100757, http://doi.org/10.1016/j.enmm.2022.100757.
19. Ethaib, S.; Al-Qutaifia, S.; Al-Ansari, N.; Zubaidi, S.L. Function of Nanomaterials in Removing Heavy Metals for Water and Wastewater Remediation: A Review. *Environments* **2022**, *9*, 123, http://doi.org/10.3390/environments9100123.
20. Elkhatib, E.A.; Moharem, M.L.; Saad, A.F.; Attia, F.A. Novel metal based nanocomposite for rapid and efficient removal of lead from contaminated wastewater sorption kinetics, thermodynamics and mechanisms. *Sci. Rep.* **2022**, *12*, 8412, http://doi.org/10.1038/s41598-022-12485-x.

21. Trache, D.; Tarchoun, A.F.; Derradji, M.; Hamidon, T.S.; Masruchin, N.; Brosse, N.; Hussin, M.H. Nanocellulose: From Fundamentals to Advanced Applications. *Front. Chem.* **2020**, *8*, 392, http://doi.org/10.3389/fchem.2020.00392.
22. Reshmy, R.; Philip, E.; Madhavan, A.; Pugazhendhi, A.; Sindhu, R.; Sirohi, R.; Awasthi, M.K.; Pandey, A.; Binod, P. Nanocellulose as green material for remediation of hazardous heavy metal contaminants. *J. Hazard. Mater.* **2022**, *424*, 127516, http://doi.org/10.1016/j.jhazmat.2021.127516.
23. Aoudi, B.; Boluk, Y.; Gamal El-Din, M. Recent advances and future perspective on nanocellulose-based materials in diverse water treatment applications. *Sci. Total Environ.* **2022**, *843*, 156903, http://doi.org/10.1016/j.scitotenv.2022.156903.
24. Shi, R.-J.; Wang, T.; Lang, J.-Q.; Zhou, N.; Ma, M.-G. Multifunctional Cellulose and Cellulose-Based (Nano) Composite Adsorbents. *Front. Bioeng. Biotechnol.* **2022**, *10*, 891034, http://doi.org/10.3389/fbioe.2022.891034.
25. Miyashiro, D.; Hamano, R.; Umemura, K. A Review of Applications Using Mixed Materials of Cellulose, Nanocellulose and Carbon Nanotubes. *Nanomaterials* **2020**, *10*, 186, http://doi.org/10.3390/nano10020186.
26. Deng, L.; Young, R.J.; Kinloch, I.A.; Abdelkader, A.M.; Holmes, S.M.; De Haro-Del Rio, D.A.; Eichhorn, S.J. Supercapacitance from Cellulose and Carbon Nanotube Nanocomposite Fibers. *ACS Appl. Mater. Interfaces* **2013**, *5*, 9983–9990, http://doi.org/10.1021/am403622v.
27. Aziz, T.; Farid, A.; Haq, F.; Kiran, M.; Ullah, A.; Zhang, K.; Li, C.; Ghazanfar, S.; Sun, H.; Ullah, R.; Ali, A.; Muzammal, M.; Shah, M.; Akhtar, N.; Selim, S.; Hagagy, N.; Samy, M.; Al Jaouni, S.K. A Review on the Modification of Cellulose and Its Applications. *Polymers* **2022**, *14*, 3206, http://doi.org/10.3390/polym14153206.
28. Elsayad, K.; Urstöger, G.; Czibula, C.; Teichert, C.; Gumulec, J.; Balvan, J.; Pohlt, M.; Hirn, U. Mechanical Properties of cellulose fibers measured by Brillouin spectroscopy *Cellulose* **2020**, *27*, 4209–4220, http://doi.org/10.1007/s10570-020-03075-z.
29. Rahaman, H.; Islam, A.; Islam, M.; Rahman, A.; Alam, S.M.N. Biodegradable composite adsorbent of modified cellulose and chitosan to remove heavy metal ions from aqueous solution. *Curr. Res. Green Sustain. Chem.* **2021**, *4*, 100119, http://doi.org/10.1016/j.crgsc.2021.100119.
30. Daochalermwong, A.; Chanka, N.; Songsrirote, K.; Dittanet, P.; Niamnuy, C.; Seubsai, A. Removal of Heavy Metal Ions Using Modified Celluloses Prepared from Pineapple Leaf Fiber. *ACS Omega* **2020**, *5*, 5285–5296, http://doi.org/10.1021/acsomega.9b04326.
31. Zhan, W.; Xu, C.; Qian, G.; Huang, G.; Tang, X.; Lin, B. Adsorption of Cu(II), Zn(II), and Pb(II) from aqueous single and binary metal solutions by regenerated cellulose and sodium alginate chemically modified with polyethyleneimine. *RSC Adv.* **2018**, *8*, 18723–18733, http://doi.org/10.1039/C8RA02055H.
32. O'Connell, D.W.; Birkinshaw, C.;O'Dwyer, T.F Heavy metal adsorbents prepared from the modification of cellulose: A review. *Bioresour. Technol.* **2008**, *99*, 6709–6724, http://doi.org/10.1016/j.biortech.2008.01.036.
33. Barker, D.; Fors, A.; Lindgren, E.; Olesund, A.; Schröder, E. Filter function of graphene oxide: Trapping perfluorinated molecules. *J. Chem. Phys.* **2020**, *152*, 024704, http://doi.org/10.1063/1.5132751.
34. Tobón, L.L.A.; Branda, M.M. Predicting the adsorption capacity of iron nanoparticles with metallic impurities (Cu, Ni and Pd) for arsenic removal: a DFT study. *Adsorption* **2020**, *26*, 127–139, http://doi.org/10.1007/s10450-019-00177-4.
35. Guo, F.; Xu, J.; Fein, J.B.; Huang, Q.; Rong, X. Crystal face-dependent methylmercury adsorption onto mackinawite (FeS) nanocrystals: A DFT-D3 study. *Chem. Eng. J.* **2021**, *420*, 127594, http://doi.org/10.1016/j.cej.2020.127594.
36. Dzade, N.Y.; Roldan, A.; de Leeuw, N.H. Structures and Properties of $As(OH)_3$ Adsorption Complexes on Hydrated Mackinawite (FeS) Surfaces: A DFT-D2 Study. *Environ. Sci. Technol.* **2017**, *51*, 3461-3470, http://doi.org/10.1021/acs.est.7b00107.
37. Liu, Y.; Liu, H.; Shen, Z. Nanocellulose Based Filtration Membrane in Industrial Waste Water Treatment: A Review. *Materials* **2021**, *14*, 5398, http://doi.org/10.3390/ma14185398.
38. Ezzat, H.; Menazea, A.A.; Omara, W.; Basyouni, B.H.; Helmy, S.A.; Mohamed, A.A.; Tawfik, W.; Ibrahim, M. DFT: B3LYP/LANL2DZ Study for the Removal of Fe, Ni, Cu, As, Cd and Pb with Chitosan. *Biointerface Res. Appl. Chem.* **2020**, *10*, 7002-7010, http://doi.org/10.33263/BRIAC106.70027010.
39. Reis, D.T.; Ribeiro, I.H.S.; Pereira, D.H. DFT study of the application of polymers cellulose and cellulose acetate for adsorption of metal ions (Cd^{2+}, Cu^{2+} and Cr^{3+}) potentially toxic. *Polym. Bull.* **2020**, *77*, 3443–3456, http://doi.org/10.1007/s00289-019-02926-5.

40. Jha, S.K.; Roth, M.; Todde, G.; Buchanan, J.P.; Moser, R.D.; Shukla, M.K.; Subramanian, G. Role of Stone-Wales Defects on the Interfacial Interactions among Graphene, Carbon Nanotubes, and Nylon 6: A First-Principles Study. *J. Chem. Phys.* **2018**, *149*, 054703, http://doi.org/10.1063/1.5032081.
41. Ahangari, M.G.; Fereidoon, A.; Ganji, M.D. Density functional theory study of epoxy polymer chains adsorbing onto single-walled carbon nanotubes: electronic and mechanical properties. *J. Mol. Model.* **2013**, *19*, 3127-3134, http://doi.org/10.1007/s00894-013-1852-6.
42. Jelil, J.; Abdurahman, A.; Gülseren, O.; Schwingenschlögl, U. Non-covalent functionalization of single wall carbon nanotubes and graphene by a conjugated polymer. *Appl. Phys. Lett.* **2014**, *105*, 013103, http://doi.org/10.1063/1.4886968.
43. Shen, Y.; Yang, X.; Bian, Y.; Nie, K.; Liu, S.; Tang, K.; Zhang, R.; Zheng, Y.; Gu, S. First-principles insights on the electronic and optical properties of ZnO@CNT core@shell nanostructure. *Sci. Rep.* **2018**, *8*, 15464, http://doi.org/10.1038/s41598-018-33991-x.
44. Zhu, B.; Wang, K.; Sun, W.; Fu, Z.; Ahmad, H.; Fan, M.; Gao, H. Revealing the adsorption energy and interface characteristic of cellulose-graphene oxide composites by first-principles calculations. *Compos. Sci. Technol.* **2022**, *218*, 109209, http://doi.org/10.1016/j.compscitech.2021.109209.
45. Hohenberg, P.; Kohn, W. Inhomogeneous Electron Gas. *Phys. Rev.* **1964**, *136*, B864, http://doi.org/10.1103/PhysRev.136.B864.
46. Perdew, J.P.; Burke, K.; Ernzerhof, M. Generalized Gradient Approximation Made Simple. *Phys. Rev. Lett.* **1996**, *77*, 3865, http://doi.org/10.1103/PhysRevLett.77.3865.
47. Hamann, D.R. Optimized norm-conserving Vanderbilt pseudopotentials. *Phys. Rev. B* **2013**, *88*, 085117, http://doi.org/10.1103/PhysRevB.88.085117.
48. Grimme, S.; Hansen, A.; Brandenburg, J.G.; Bannwarth, C. Dispersion-Corrected Mean-Field Electronic Structure Methods. *Chem. Rev.* **2016**, *116*, 5105–5154, http://doi.org/10.1021/acs.chemrev.5b00533.
49. Giannozzi, P.; Baroni, S.; Bonini, N.; Calandra, M.; Car, R.; Cavazzoni, C.; Ceresoli, D.; Chiarotti, G.L.; Cococcioni, M.; Dabo, I.; Dal Corso, A.; de Gironcoli, S.; Fabris, S.; Fratesi, G.; Gebauer, R.; Gerstmann, U.; Gougoussis, C.; Kokalj, A.; Lazzeri, M.; Martin-Samos, L.; Marzari, N.; Mauri, F.; Mazzarello, R.; Paolini, S.; Pasquarello, A.; Paulatto, L.; Sbraccia, C.; Scandolo, S.; Sclauzero, G.; Seitsonen, A.P.; Smogunov, A.; Umari, P.; Wentzcovitch, R.M. QUANTUM ESPRESSO: a modular and open-source software project for quantum simulations of materials. *J. Phys. Condens. Matter* **2009**, *21*, 395502, http://doi.org/10.1088/0953-8984/21/39/395502.
50. Giannozzi, P.; Baseggio, O.; Bonfà, P.; Brunato, D.; Car, R.; Carnimeo, I.; Cavazzoni, C.; de Gironcoli, S.; Delugas, P.; Ruffino, F.F.; Ferretti, A.; Marzari, N.; Timrov, I.; Urru, A.; Baroni, S. Quantum ESPRESSO toward the exascale. *J. Chem. Phys.* **2020**, *152*, 154105, http://doi.org/10.1063/5.0005082.
51. Koumpouras, K.; Larsson, J.A. Distinguishing between chemical bonding and physical binding using electron localization function (ELF). *J. Phys.: Condens. Matter* **2020**, *32*, 315502, http://doi.org/10.1088/1361-648X/ab7fd8.
52. Becke, A.D.; Edgecombe, K.E. A simple measure of electron localization in atomic and molecular systems. *J. Chem. Phys.* **1990**, *92*, 5397–5403, http://doi.org/10.1063/1.458517.
53. Henkelman, G.; Arnaldsson, A.; Jónsson, H. A fast and robust algorithm for Bader decomposition of charge density. *Comput. Mater. Sci.* **2006**, *36*, 354–360, http://doi.org/10.1016/j.commatsci.2005.04.010.
54. Tang, W.; Sanville, E.; Henkelman, G. A grid-based Bader analysis algorithm without lattice bias. *J. Phys.: Condens. Matter* **2009**, *21*, 084204, http://doi.org/10.1088/0953-8984/21/8/084204.
55. Sanville, E.; Kenny, S.D.; Smith, R.; Henkelman, G. Improved grid-based algorithm for Bader charge allocation. *J. Comput. Chem.* **2007**, *28*, 899–908, http://doi.org/10.1002/jcc.20575.
56. Nishiyama, Y.; Sugiyama, J.; Chanzy, H.; Langan, P. Crystal Structure and Hydrogen Bonding System in Cellulose I_α from Synchrotron X-Ray and Neutron Fiber Diffraction. *J. Am. Chem. Soc.* **2003**, *125*, 14300–14306, http://doi.org/10.1021/ja037055w.
57. Nishiyama, Y.; Langan, P.; Chanzy, H. Crystal Structure and Hydrogen-Bonding System in Cellulose Iβ from Synchrotron X-Ray and Neutron Fiber Diffraction. *J. Am. Chem. Soc.* **2002**, *124*, 9074–9082, http://doi.org/10.1021/ja0257319.
58. Pido, A.A.G.; Munio, A.A.Z.; Ambolode II, L.C.C. *Ab Initio* Calculations of the Atomic Structure, Stability, and Electronic Properties of $(C_6H_{10}O_5)_2$ Encapsulation into Hydrogen-Doped Carbon Nanotube. *Nano Hybrids Composites* **2023**, *38*, 53–62, http://doi.org/10.4028/p-3uk80a.

59. Madabeni, A.; Dalla Tiezza, M.; Omage, F.B.; Nogara, P.A.; Bortoli, M.; Rocha, J.B.T.; Orian, L. Chalcogen–mercury bond formation and disruption in model Rabenstein's reactions: A computational analysis. *J. Comput. Chem.* **2020**, *41*, 2045–2054, http://doi.org/10.1002/jcc.26371.
60. Deshpande, M.D.; Scheicher, R.H.; Ahuja, R.; Pandey, R. Binding Strength of Sodium Ions in Cellulose for Different Water Contents. *J. Phys. Chem. B* **2008**, *112*, 8985–8989, http://doi.org/10.1021/jp8020547.